Role of Aromatic Residues at the Lipid−Water Interface in Micelle-Bound Bacteriophage M13 Major Coat Protein†

Christopher T. K. Yuen,‡,§ Alan R. Davidson,§,|| and Charles M. Deber*,‡,§

Division of Structural Biology and Biochemistry, Research Institute, Hospital for Sick Children, 555 University Avenue, Toronto, Ontario, Canada M5G 1X8, Department of Biochemistry, University of Toronto, Toronto, Ontario, Canada M5S 1A8, and Department of Molecular Genetics and Microbiology, University of Toronto, Toronto, Ontario, Canada M5S 1A8

Received July 11, 2000

ABSTRACT: Analyses of transmembrane domains of proteins have revealed that aromatic residues tend to cluster at or near the lipid−water interface of the membrane. To assess protein−membrane interactions of such residues, a viable mutant library was generated of the major coat protein of bacteriophage M13 (a model single membrane-spanning protein) in which one or the other of its interfacial tyrosine residues (Tyr-21 and Tyr-24) is mutated. Using the interfacial tryptophan (Trp-26) as an intrinsic probe, blue shifts in fluorescence emission spectra and quenching constants indicated that mutants with a polar amino acid substitution (such as Y24D or Y24N) are less buried in a deoxycholate micelle environment than in the wild type protein. These polar mutants also exhibited α-helix to β-structure transition temperatures in incremental-heating circular dichroism studies relatively lower than those of wild type and nonpolar mutants (such as Y21V, Y21I, and Y24A), indicating that specific side chains in the lipid−water interface influence local protein−micelle interactions. Mutant Y21F exhibited the highest transition temperature, suggesting that phenylalanine is ostensibly the most effective interfacial anchoring residue. Using phage viability as the assay in a combination of site-directed and saturation mutagenesis experiments, it was further observed that both Tyr residues could not simultaneously be "knocked out". The overall results support the notion that an interfacial Tyr is a primary recognition element for precise strand positioning in vivo, a function that apparently cannot be performed optimally by residues with simple aliphatic character.

Several families of membrane proteins, including anion exchangers, bacterial multidrug resistance proteins, and bacteriorhodopsin, have a preponderance of aromatic residues at or near the membrane−water interface of their transmembrane (TM)[1] helices (*1*, *2*). Studies on a variety of membrane proteins have indicated that Trp and Tyr are enriched in extracytoplasmic segments and at the ends of TM helices (*3*). High-resolution structures of membrane proteins provide further evidence of clustering of aromatic residues at the membrane−water interface of TM domains, whether the domains are α-helical or β-sheet in structure (*4*). Localization of aromatic amino acids is also observed in photosynthetic reaction centers (*5*), the potassium channel from *Streptomyces lividans* (*6*) and bacterial porins (*7*). A variety of roles have been proposed for interfacial aromatic residues, including positioning or anchoring the TM segments in the membrane (*8*), introducing rigidity to the periphery of TM segments (*1*), allowing vertical mobility of the TM region with respect to the membrane (*9*), facilitating translocation of the periplasmic portion of protein through the membrane, and acting as determinants of protein orientation (*10*). Trp was also shown to influence the positioning of a poly-Leu TM segment in a microsomal membrane (*11*).

We focus here on aromatic residues of membrane proteins at the membrane−water interface, and examine their influence on protein−lipid interactions of the adjoining TM segment. For these studies, the major coat protein (pVIII) of filamentous bacteriophage M13 was chosen as a prototypical single membrane-spanning protein (for reviews of the bacteriophage and the protein, see refs *12*−*16*). This 50-residue, 5.2 kDa protein (AEGDDPAKAAFNSLQASATEYIGYAWAMVVVIVGATIGIKLFKKFTSKAS) (*17*) is encoded by gene VIII of the viral DNA and is the main component of the phage particle; 2700 copies are bound to the viral DNA in each phage particle, comprising 98% of the total protein mass or 86% of the total mass of the phage (*13*, *18*, *19*). During infection, it exists as a stably inserted type I single membrane-spanning protein in the inner membrane of *Escherichia coli* (*20*). The sequence of M13 major coat protein is identical to that of bacteriophages fd and f1 except at position 12 (Asn in M13 and Asp in fd and f1) (*17*). It adopts mainly α-helical conformations in both DNA- and membrane-bound forms (*19*). Results from several biophysical studies in micellar environments suggest a "two-

† Supported, in part, by grants to C.M.D. and A.R.D. from the Canadian Institutes of Health Research (CIHR). C.T.K.Y. held an Ontario Graduate Scholarship.

* To whom correspondence should be addressed at the Research Institute, Hospital for Sick Children. E-mail: deber@sickkids.on.ca.

‡ Hospital for Sick Children.

§ Department of Biochemistry, University of Toronto.

|| Department of Molecular Genetics and Microbiology, University of Toronto.

[1] Abbreviations: CD, circular dichroism; CMC, critical micelle concentration; dNTP, deoxynucleoside triphosphate; DOC, deoxycholate; PAGE, polyacrylamide gel electrophoresis; PCR, polymerase chain reaction; SDS, sodium dodecyl sulfate; TM, transmembrane; WT, wild type.

10.1021/bi0016117 CCC: $19.00
Published on Web 12/19/2000

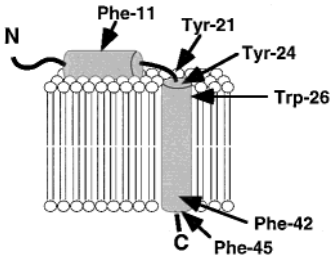

FIGURE 1: Bacteriophage M13 major coat protein in the membrane, with the approximate locations of the six aromatic residues shown. The "L-shaped" model shown, consisting of an N-terminal amphipathic surface helix and a micelle-spanning C-terminal helix, has been deduced from biophysical studies of the structure of micelle-bound M13 coat protein (*21*, *22*, *25*) and the related bacteriophage Ike coat protein (*63*).

helix" model for membrane-associated coat protein (Figure 1): a TM helix that enters the membrane between residues 25 and 27 and exits between residues 44 and 46 (*21*−*25*) and an amphipathic helix, likely embedded in the micellar surface, that occurs between residues 8 and 16 (*25*). The particular advantage of M13 coat protein for this work is that of the six aromatic residues in the protein, five of them (Tyr-21, Tyr-24, Trp-26, Phe-42, and Phe-45) are at or near the membrane−water interface deduced for the membrane-bound form of the protein (Figure 1).

Large-scale production (milligram amounts) of M13 major coat protein is readily performed from phage growth and purification (*26*). While a library of about 100 viable mutants over the full protein sequence has been generated by our laboratory (*27*), these mutagenesis experiments have been unable to generate viable mutants with Phe-11, Trp-26, Phe-42, and Phe-45 substituted. In contrast, the two interfacial aromatic residues (Tyr-21 and Tyr-24) can be substituted with many charged, polar, or nonpolar residues without compromising the viability of the phage, thus presenting an excellent opportunity to assess the specific interfacial role(s) for these latter residues. In the work presented here, wild type (WT) coat protein and viable mutants with either Tyr mutated are compared on the basis of their protein−lipid interactions in a micellar environment. The effects of this manipulation of interfacial Tyr residues are probed through fluorescence studies, and through circular dichroism (CD) measurements of the rate of mutant-dependent heat-induced α-helix to β-structure conformational transitions.

MATERIALS AND METHODS

Mutagenesis. Oligonucleotide-directed saturation mutagenesis experiments were performed as previously described using the Sculptor *in vitro* mutagenesis system (Amersham) to produce viable mutants of bacteriophage M13 major coat protein with Tyr-21 and/or Tyr-24 substituted (*26*, *27*). The oligonucleotide used in the double-site saturation mutagenesis had the sequence 5′-CAACCATCGCCCACGCNNNAC-CGATNNNTTCGGTCGCTGAGGC-3′, where N is 25% of each nucleotide. The product of mutagenesis (repolymerized double-stranded DNA) was transformed into *E. coli* JM101 competent cells. The resultant phage plaques were subjected to single-stranded DNA isolation, and the DNAs were screened by sequencing for mutants.

PCR Amplification of Mutagenesis Products. To confirm that the mutagenesis product (i.e., the repolymerized double-stranded DNA) being transformed did carry the desired nucleotide base changes, the portion containing gene VIII was amplified by polymerase chain reaction (PCR) with a 1:50 dilution of the mutagenesis product as the template and *Pfu* DNA polymerase (Stratagene) as the enzyme. The upper PCR primer had the sequence 5′-GCCTCTTTCGTTTTAG-GTTGGTGCC-3′, and the lower primer had the sequence 5′-CAACAGTTTCAGCGGAGTGAGAATAG-3′. The desired PCR product had 416 base pairs, which included the entire coding sequence for gene VIII. The 100 μL reaction mixture consisted of cloned *Pfu* DNA polymerase (2.5 units), DNA template (100 ng), primers (250 ng each), the four dNTPs (25 mM each), and 10 μL of 10× cloned *Pfu* DNA polymerase reaction buffer (Stratagene). It was overlaid with 50 μL of mineral oil. The thermal cycler that was used was the OmniGene Thermal Cycling System (Hybaid). The cycling parameters were as follows: (1) one cycle at 95 °C for 45 s, (2) 25 cycles at 95 °C for 45 s, 55.8 °C for 45 s, and 72 °C for 90 s, and (3) one cycle at 72 °C for 10 min. The annealing temperature (55.8 °C) was determined using the following equation (*28*):

$$T_{\text{anneal}} = 0.3T_{\text{m}}(\text{primer}) + 0.7T_{\text{m}}(\text{product}) - 14.9\ ^{\circ}\text{C}$$

where T_{anneal} is the annealing temperature and T_{m} is the melting temperature. The PCR product was purified by the QIAquick PCR purification kit (QIAGEN) and subjected to DNA sequencing at the ACGT Corp. (Toronto, ON).

Protein Sample Preparation. WT and mutant phages were amplified by infecting 1 L cultures of *E. coli* JM101 in 2× TY medium (1.6% tryptone, 1% yeast extract, and 0.5% NaCl). Phage was obtained by precipitation with 0.2 volume of 20% poly(ethylene glycol) 8000 and 2.5 M NaCl. After overnight incubation at 4 °C, the supernatant was centrifuged for 30 min at 10 000 rpm. The viral pellet was resuspended in TE buffer (1 mL). This phage stock (10 mg) was then shaken at 200 rpm at 37 °C when mixed with 2 volumes of extract solution [0.1 M ammonium bicarbonate and 70 mM sodium deoxycholate (pH 9.0)] and 1 volume of chloroform. One further volume of chloroform was added after 30 min, and shaking was continued until all the chloroform evaporated. Then, the major coat protein was purified from DNA by gel filtration using a Sephacryl S-200 high-resolution column (Pharmacia) equilibrated with 8 mM sodium deoxycholate and 25 mM sodium borate (pH 9.0). All subsequent experiments were performed starting with stock solutions of the WT and mutant proteins (1 mg/mL) in 30 mM sodium deoxycholate and 25 mM sodium borate (pH 9.0).

SDS−*PAGE*. Sodium dodecyl sulfate−polyacrylamide gel electrophoresis (SDS−PAGE) was carried out using NOVEX precast 10 to 20% Tricine gels. Protein samples (5 μg each) were heated at different temperatures before the addition of the Tricine SDS sample buffer (NOVEX), but they were not subsequently boiled. For experiments involving 2-mercaptoethanol, the reagent (1 μL) was incubated with the protein for 15 min before the addition of sample buffer.

Fluorescence Emission and Quenching. Experiments were carried out using a Photon Technology International QM-1 fluorescence spectrometer. Typically, 3 μM protein (2 mL) was placed in an acrylic cuvette with a path length of 1 cm. The excitation wavelength was set at 295 nm to selectively excite Trp, and the emission spectrum was recorded from

300 to 400 nm. Three independent scans were performed for each protein. In fluorescence quenching experiments, 8 M acrylamide was added to samples, yielding 3 μM protein with various concentrations of acrylamide. The fluorescence emission spectra were recorded similarly as were those for the samples for emission measurements.

Incremental-Heating CD Experiments. CD spectra of protein samples subjected to incremental heating were recorded using a JASCO J-720 spectropolarimeter. Samples (1 mg/mL protein) were placed in a cylindrical water-jacketed quartz cell with a path length of 0.01 cm. Samples were heated from 25 to 95 °C with a 5 min incubation at every 5 °C interval, and spectra were recorded at the end of each incubation. Each spectrum was the average of four scans between 250 and 190 nm with noise reduction and baseline subtraction applied.

Constant-Heating CD Experiments. Measurements were carried out with an Aviv 62A DS CD spectrometer. Protein samples (0.1 mg/mL) were placed in a rectangular quartz cell with a path length of 0.1 cm, heated from 25 to 95 °C within 2.5 min, and maintained at 95 °C for the duration of the experiment. The α-helical parameter, ellipticity at 208 nm (θ_{208}), was monitored for 1 h from the start of heating.

RESULTS

Mutagenesis. Through randomized mutagenesis using the Eckstein method (*29*), phage stocks were available in this laboratory for several single-site viable M13 coat protein mutants at Tyr-24 (Y24A, Y24D, and Y24N) (*26*, *30*) and at Tyr-21 (Y21F, Y21I, Y21T, and Y21V; T. Neogi, M. Glibowicka, and C. M. Deber, unpublished results). Also, to investigate the full range of viable mutants that can be obtained in this region of the protein, we carried out additional saturation mutagenesis experiments designed specifically to generate double-site mutants where both Tyr-21 and Tyr-24 are replaced simultaneously with other residues. It is emphasized that these experiments can produce only viable mutants, viz., those that can be synthesized, processed, and incorporated into the bacteriophage successfully in vivo. Notwithstanding extensive attempts using several types of oligonucleotide templates (e.g., with Y21 and Y24 positions both randomized, with Y21I with Y24 randomized, and/or with Y21F with Y24 randomized) and through varying the oligonucleotide:template ratio and/or the polymerase that was used (T7 or Klenow), we found that no such viable double-site mutants with both Tyr residues replaced could be obtained (although several mutant DNAs contained a mutation at one site and a silent mutation at the other site). In any case, the variety of viable nonpolar and polar substitutions obtained at Tyr-21 and Tyr-24 provides de facto evidence that neither of the Tyr residues plays a determining role in those protein−protein interactions which significantly influence packing in the virion structure, and accordingly whose function may be localized to membrane-related events in the phage life cycle.

Saturation mutagenesis procedures did lead to two mutants, Y24C and S17L/Y24D, which had not been discovered in previous studies. The fact that a viable Y24C mutant was isolated appears to suggest that a built-in mechanism exists on the part of the phage to prevent self-association during assembly. It is possible that the membrane at the phage assembly site is reducing in vivo, thereby preventing formation of disulfide bonds. As well, it has been proposed that phage proteins pI and pXI promote dissociation of oligomerized major coat proteins prior to their incorporation into the virion (*31*).

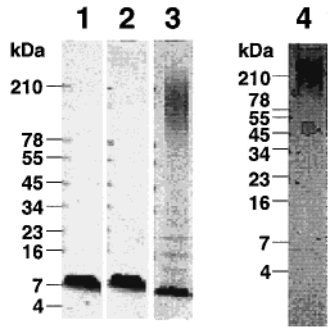

FIGURE 2: SDS−PAGE analysis of wild type M13 bacteriophage major coat protein. Protein (5 μg) was loaded in 30 mM sodium deoxycholate and 25 mM sodium borate (pH 9.0) and incubated (lane 1) at 25 °C for 1 h, (lane 2) at 65 °C for 1 h, (lane 3) at 95 °C for 5 min, or (lane 4) at 95 °C for 90 min.

In a further assessment of the outcome of the mutagenesis procedures, we sequenced the PCR product of the relevant segment of the mutagenesis product (see Materials and Methods). All four nucleotides were found to be present at all six base positions corresponding to residues 21 and 24 of the major coat protein (not shown), demonstrating that the bases had indeed been randomized and indicating the potential for mutants at these sites had they been viable. Thus, in combination with the mutagenesis studies described above, it was concluded that the essentially complete viable mutant library in this region of the M13 major coat protein had been obtained.

SDS−PAGE. To assess initially the oligomeric state of the mutants under different temperatures, WT and mutant coat proteins, as obtained directly from purification by gel filtration in deoxycholate-containing media, were heated at 25 (for 1 h), 65 (for 1 h), and 95 °C (for 5 min or for 90 min) and then analyzed by SDS−PAGE (Figure 2). All proteins, with the exception of Y24C, were almost exclusively monomeric after incubations at 25 and 65 °C. The Y24C mutant protein was dimeric due to spontaneous formation of a disulfide bond, which could be reduced with the addition of 2-mercaptoethanol (not shown). As known for the heat-induced $\alpha \rightarrow \beta$ transition of micelle-bound M13 coat protein (*32*), SDS-resistant aggregated (β) protein was present after a 5 min incubation at 95 °C and was the dominant species after 90 min at 95 °C for all proteins.

Fluorescence Emission. On the basis of micelle-bound structures deduced for M13 major coat protein (*21*−*25*), its single Trp residue (Trp-26) is located just inside the hydrophobic interior of the lipid environment, making it convenient to correlate any red shift in the fluorescence emission maximum with changes in the positioning (i.e., toward a more aqueous microenvironment) of the TM segment with respect to the micelle. The excitation wavelength was set at 295 nm to selectively excite Trp but not Tyr (*33*). From these experiments, we found that WT and mutant major coat proteins in deoxycholate (DOC) micelles can be roughly divided into two groups based on their fluorescence emission (Figure 3 and Table 1). The first group, consisting of WT, the Y21 mutants, and Y24A, had higher fluorescence intensities and shorter wavelengths at their

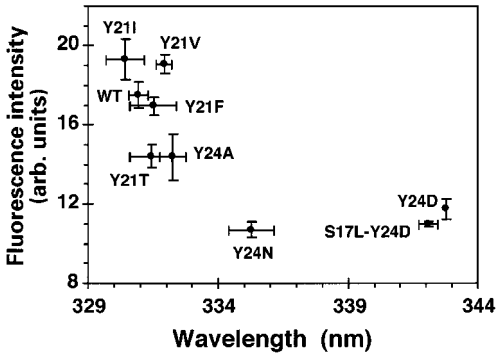

FIGURE 3: Plot of the maximum fluorescence emission intensities against maximum emission wavelengths of the WT M13 coat protein and mutant proteins. The excitation wavelength was set at 295 nm to selectively excite Trp-26. The protein concentration was 3 μM in 30 mM sodium deoxycholate and 25 mM sodium borate (pH 9.0).

Table 1: Fluorescence Emission Maxima (excitation wavelength of 295 nm), and $\alpha \rightarrow \beta$ Transition Temperatures in Incremental-Heating CD Experiments of WT and Mutant M13 Major Coat Proteins[a]

protein	λ_{max} (nm)[b]	transition temperature (°C)[c]
WT	331	79.8
Y21F	332	82.3
Y21I	330	80.3
Y21T	331	79.2
Y21V	332	78.2
Y24A	332	78.1
Y24D	343	69.4
S17L/Y24D	342	73.0
Y24N	335	77.0

[a] Fluorescence experiments were carried out with 3 μM protein in 30 mM sodium deoxycholate and 25 mM sodium borate (pH 9.0). Incremental-heating CD experiments were performed with 1 mg/mL protein in 30 mM sodium deoxycholate and 25 mM sodium borate (pH 9.0). [b] The average error is 0.6 nm. [c] The average error is 0.3 °C.

emission maxima, whereas the second group, consisting of the Y24 mutants which have polar or charged side chains, typically had much lower intensities and longer wavelengths.

Fluorescence Quenching. Acrylamide was used to probe the degree of exposure of Trp-26 in WT and mutant major coat proteins solubilized in deoxycholate micelles. As a polar molecule, acrylamide will not penetrate into the hydrophobic interior of the micelles and is therefore expected to quench the more exposed Trp more effectively. Plotting F_0/F, where F_0 is the unquenched fluorescence intensity and F is the quenched fluorescence intensity, against quencher concentration [Q] (in molar) (curves not shown) generated upward-curving lines between 0 and 0.8 M for all proteins, indicating that not all of the quenching was due to dynamic quenching caused by collision of the quencher and the Trp residue, which is the fluorophore (*34*). Static quenching arises from the proximity of quencher molecules to the Trp at the moment of excitation, leading to instantaneous quenching (*35*). To account for both dynamic and apparent static quenching (i.e., static quenching without complex formation between the quencher and the fluorophore), the results were fitted to the modified Stern−Volmer equation:

$$\frac{F_0}{F} = (1 + K_{SV}[Q])e^{V[Q]}$$

Table 2: Quenching Constants of Wild Type and Mutant M13 Major Coat Proteins[a]

protein	K_{SV} (M^{-1})	V (M^{-1})
WT	10.3 ± 0.8	0.37 ± 0.17
Y21F	9.2 ± 1.4	0.54 ± 0.27
Y21I	8.5 ± 0.3	0.61 ± 0.01
Y21T	10.6 ± 2.1	0.59 ± 0.15
Y21V	9.0 ± 0.2	0.67 ± 0.01
Y24A	7.1 ± 0.3	0.79 ± 0.07
Y24D	9.1 ± 0.3	0.96 ± 0.06
S17L/Y24D	7.5 ± 2.3	1.23 ± 0.57
Y24N	7.5 ± 0.1	1.06 ± 0.10

[a] Protein was at a concentration of 3 μM in 30 mM sodium deoxycholate and 25 mM sodium borate (pH 9.0) with varying concentrations (0−0.8 M) of acrylamide. The experimental data were fitted to a modified Stern−Volmer equation. The dynamic quenching constant (K_{SV}) and static quenching constant (V) were calculated with KaleidaGraph software for each protein in each trial.

where K_{SV} is the Stern−Volmer dynamic quenching constant (in M^{-1}) and V is the static quenching constant (in M^{-1}) (*34*). The two quenching constants are given for the full set of mutants in Table 2. We observed that mutants with a polar or charged amino acid substitution at position 24 (Y24D, S17L/Y24D, and Y24N) typically displayed greater levels of quenching, and especially greater levels of static quenching. This is a result of a relatively higher degree of Trp exposure to the aqueous environment in these mutants. In comparison, the other major coat proteins that were studied had similar or higher dynamic quenching constants (K_{SV}) but much lower static quenching constants (V), meaning that most quencher molecules had to diffuse a short distance to reach Trp to bring about dynamic quenching. Fluorescence quenching experiments using acrylamide thus confirm the findings of fluorescence emission experiments.

Micelle-Based Studies in Deoxycholate. Deoxycholate (DOC) has classically been used as a nonperturbing micelle both to extract the M13 major coat protein from bound DNA and for conformational studies (*23*, *36*−*38*). While DOC is a steroidal molecule for which micellar particles will likely deviate from the idealized spherical structures, it is believed to preserve the structure of the membrane-bound form of the coat protein (*19*, *23*). Also, the negative charge of DOC can mimic the enrichment of negatively charged phospholipids in the *E. coli* inner membrane during M13 phage infection (*32*). DOC aggregation numbers (i.e., the number of DOC monomers per micelle) have been reported as ca. 7−9 (*37*, *39*). The critical micelle concentration (CMC) of DOC and related bile salt detergents is ca. 1−3 mM (*39*, *40*), well below the concentration of 30 mM used in our circular dichroism experiments, and decreases only slightly at ≤80 °C (*39*). While some DOC monomers may remain associated hydrophobically with coat protein side chains at elevated temperatures, DOC micelles display upon heating both a decreasing tendency for monomer association (*39*) and a decreasing hydrodynamic radius of the micellar particle (*41*), both consistent with a micelle disintegration process at temperatures approaching 95 °C.

Incremental-Heating Experiments. M13 coat protein bound to DNA in the native phage particle is readily soluble in water but, upon separation from phage DNA, behaves as a water-insoluble hydrophobic protein. This phenomenon can be harnessed through the solubilization of the protein in

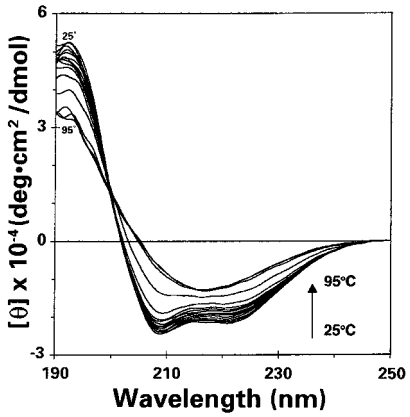

FIGURE 4: Circular dichroism spectra of WT M13 major coat protein, displaying an α-helix to *β*-sheet transition during an incremental-heating experiment. Spectra were obtained in buffer containing 30 mM sodium deoxycholate and 25 mM sodium borate (pH 9.0). The protein concentration was 1 mg/mL. Samples were heated from 25 to 95 °C with a 5 min incubation at every 5 °C interval, and spectra were recorded at the end of each incubation. See Materials and Methods for further experimental details.

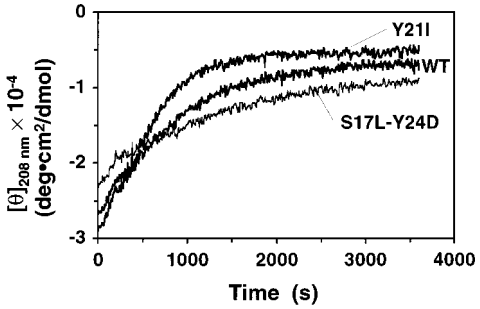

FIGURE 5: Conformational transition curves for WT and two mutant M13 major coat proteins in constant-heating CD experiments. The temperature was raised from 25 to 95 °C within 150 s and maintained at 95 °C for 1 h after the start of heating. Curves that are shown are continuous traces of protein ellipticity recorded at 10 s intervals, with the spectrometer wavelength held constant at 208 nm, during which the protein undergoes an α-helix to *β*-sheet transition. The protein concentration was 0.1 mg/mL in 30 mM sodium deoxycholate and 25 mM sodium borate (pH 9.0). See Materials and Methods for further experimental details.

detergent micelles, which generates useful systems for assessment of mutation-dependent protein−protein and protein−lipid interactions. In the incremental-heating pathway, the heating of the initial sample is stepwise, and there is ample equilibration time (12−15 min) at each cycle, viz., raising the temperature, incubating for 5 min, and recording four scans of the CD spectrum. Using this time scale, the rate-determining step is likely the mutant-dependent escape of the protein from the micelle, i.e., once the protein becomes aqueous-based and thermally denatured, self-association of the hydrophobic protein to a *β*-aggregate is expected to be rapid.

The CD spectrum of the WT major coat protein in DOC micelles at 25 °C displays the characteristic minima at 208 and 222 nm for proteins with high α-helical content; incremental heating produced a family of curves, which undergo a smooth transition to *β*-structure at elevated temperatures (Figure 4). To determine the mutation dependence of such α → *β* transition temperatures of the major coat proteins, the mean residue ellipticity at 208 nm ($[\theta]_{208}$) was plotted against the temperature at increments of 5 °C from 25 to 95 °C for each protein (not shown). Values of $[\theta]_{208}$ were used as the α-helical parameter instead of the more commonly employed $[\theta]_{222}$ because it has been shown that aromatic residues can give rise to bands near 222 nm which may interfere with the estimation of helical content (*42*). The resulting curves were sigmoidal in shape for WT and all mutants, and a clear transition from helical to *β*-type structure was apparent. A transition temperature was defined as the estimated inflection point of the sigmoidal curve where the slope reached a maximum. The α → *β* transition temperatures of the nine proteins studied ranged from 69.4 to 82.3 °C, with that of the WT at 79.8 °C (Table 1). Mutants with polar or charged substitutions at position 21 or 24 generally had lower transition temperatures than WT, with Y24D being the least thermostable. The conformational change was not reversible upon lowering of the temperature from 95 °C.

Mutation-Dependent Protein−Protein Interactions in the Aqueous Environment. Constant-Heating Experiments. While the thermally modulated α → *β* transition in micelle-bound M13 major coat protein has been widely studied and documented (*32*, *43*, *44*), relatively little information exists on the induced "*β*" state of the protein, and in particular, whether this state devolves from the actual "escape" of the protein from the micellar environment. We hypothesized that a given nascent hydrophobic protein in an aqueous environment should "aggregate" (i.e., proceed toward the *β* state) at a rate roughly correlated with the net hydrophobic character of its side chain content. To examine this situation in further detail, each major coat protein in DOC micelles was heated rapidly (within 2.5 min) in a quartz CD cuvette from 25 to 95 °C and then maintained at a constant temperature of 95 °C. The ellipticity at 208 nm (θ_{208}) was monitored for 1 h from the start of the heating. The results were plotted as mean residue ellipticity at 208 nm ($[\theta]_{208}$) versus time (Figure 5). With their slopes gradually decreasing, all plots reached their respective plateaus within 1 h. If it is assumed that the α → *β* transition is a first-order reaction and that $[\theta]_{208}(t)$ is directly proportional to the concentration of helical protein at time *t*, the data can be fitted to the following equation (C. Wang and C. M. Deber, unpublished results; see also ref *45*):

$$\ln\left(\frac{[\theta]_{208}(t) - [\theta]_{208}(\infty)}{[\theta]_{208}(0) - [\theta]_{208}(\infty)}\right) = -kt$$

where $[\theta]_{208}(t)$ is the mean residue ellipticity at 208 nm at time *t*, $[\theta]_{208}(0)$ is the most negative $[\theta]_{208}$ observed, $[\theta]_{208}(\infty)$ is the average $[\theta]_{208}$ of the last 30 data points (over the last 300 s) with two standard deviations added, *t* is the time in seconds, and *k* is the first-order rate constant in inverse seconds. Plotting the natural logarithmic function against time yields a line whose slope should be equal to −*k* (not shown). The plots for the nine major coat proteins each displayed a linear relationship up to about 1000 s. The rate constants (*k*) were thus calculated from the data between 300 and 1000 s after the start of heating (Table 3). The initial 300 s was time allowed for heating and was disregarded in the calculations. In these experiments, we noted a general reversal from trends observed by incremental heating; that is, the more nonpolar mutants at either position 21 or 24

Table 3: Rate Constants of the $\alpha \rightarrow \beta$ Transition of Proteins in Constant-Heating Circular Dichroism Experiments[a]

protein	k ($\times 10^3$ s^{-1})	protein	k ($\times 10^3$ s^{-1})
Y21V	2.17	Y21T	1.38
Y21I	1.95	WT	1.11
Y24A	1.78	S17L/Y24D	0.64
Y21F	1.64	Y24N	0.58
Y24D	1.45		

[a] The rate constants (k) are equal to the negative of the slopes of the plots of the natural logarithmic function (see the text) vs time (in seconds). The data between 300 and 1000 s were used in the calculation. The proteins are listed in descending order of their rates of conformational transition.

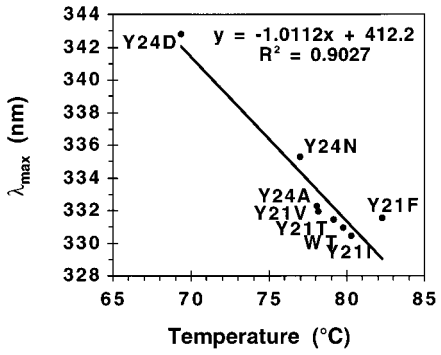

FIGURE 6: Correlation between maximum fluorescence emission wavelengths and $\alpha \rightarrow \beta$ transition temperatures of M13 major coat proteins as measured by incremental-heating CD experiments. S17L/Y24D, a double-site mutant, is excluded from the plot.

tended to undergo the $\alpha \rightarrow \beta$ transition more quickly. For example, Y24N and S17L/Y24D had the slowest rates of conformational change and were the most stable at 95 °C.

DISCUSSION

While both incremental-heating and constant-heating (at 95 °C) CD experiments performed herein measure an apparent "rate" of the conformational transition of the major coat proteins, the information obtained in each type of experiment is different. The varying events measured by the two types of experiments constitute the net process of the α-helix to β-structure transition. Whichever protocol is used, heating eventually overcomes extant protein−lipid interactions and causes the protein to escape from the micelle into the aqueous environment. In incremental-heating experiments, we found a sequence−temperature functional relationship, with a range of $\alpha \rightarrow \beta$ transition temperatures (ca. 69 to 82 °C) (Table 1) in which the most polar mutants (noticeably Y24D, S17L/Y24D, and Y24N) had the lowest transition temperatures. SDS−PAGE gel experiments confirmed that the heating process is accompanied by coat protein aggregation. Since the incremental-heating experiments fundamentally elucidate protein−lipid interactions, the fact that the transition temperature in mutant-dependent reinforces the notion of the Tyr-21−Tyr-24 segment being in a membrane−water interfacial region, but where nonpolar side chains retain access to the lipid core of the micelle, and therefore contribute toward determining the observed transition temperatures. A plot of maximum fluorescence emission wavelengths against transition temperatures (Figure 6) gave a linear correlation between the two parameters, a result further suggesting that the observed transition temperature dependence is lipid-based.

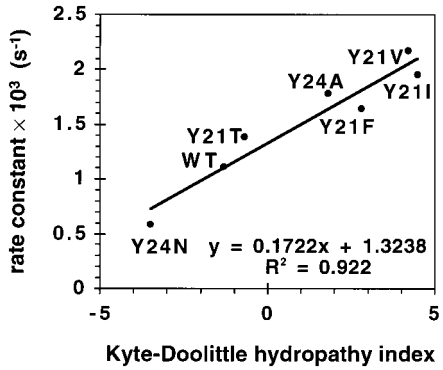

FIGURE 7: Correlation between rate constants (k) obtained for M13 major coat proteins in constant-heating CD experiments (95 °C) and the Kyte−Doolittle hydropathy scale. Because of possible charge effects, S17L/Y24D and Y24D were excluded from the plot.

An inverse correlation arose in the constant-heating CD experiments, where rate constants (k) confirm that here the mutation-dependent association of the protein monomers becomes water-based, viz., while the nonpolar mutants escape the micelle relatively slowly, they then aggregate more quickly, a manifestation of the hydrophobic effect in the aqueous environment. Indeed, a plot of the rate constants obtained for aggregation at 95 °C against the Kyte−Doolittle hydropathy index (*46*), a scale derived mainly from structural data of water-soluble proteins, reveals a linear correlation (Figure 7), affirming the dependence of aggregation on sequence context. Interestingly, the rate constant observed for Y21F is below that of mutants containing V, I, and A, and that for WT (Y) itself is below all of these and also a mutant containing T. This observation of relatively diminished hydrophobic character for Phe and Tyr in aqueous medium is in contrast to the high hydrophobicity displayed by these residues in scales measuring transfer of peptides from aqueous to membrane environments (*47*, *48*). These latter results indicate a dual or amphiphilic nature for aromatic residues, which likely imparts to them the adaptability required for interactions at the membrane−water interface.

The fluorescence emission maximum is a reliable marker for the environment of a Trp residue in a protein, including its relative penetration into a membrane environment (*49*). The facts that (1) all proteins (excluding Y24C) that have been studied are monomeric on SDS−PAGE gels at room temperature (wild type, Figure 2; others not shown) and (2) all proteins display highly helical CD spectra in DOC micelles at 25 °C, further validate the use of Trp-26 fluorescence as a probe of the protein position in the micelle. The results of fluorescence emission experiments demonstrate that the position of Trp-26 relative to the hydrophobic interior of the DOC micelle can be affected by the nature of residues at positions 21 and 24 (Table 1). Thus, the local polarity of Trp-26 increases with a polar or charged residue at either position, but Trp-26 becomes more "buried" in the micelle with a more hydrophobic substitution of Tyr. This is true whether the nonpolar substitution is at Tyr-21 (Y21I and Y21V) or at Tyr-24 (Y24A). WT and Y21F exhibited similar emission maxima and intensity due to their common aromatic character at the interface. Y21T and Y24A are another pair of proteins that share fluorescence emission properties, which agrees with the similar ranking of Ala and Thr on several hydrophobicity scales (*47*, *48*, *50*). While CD spectra of the

nonpolar mutants in the present protein library did display a perceptible trend toward relatively greater negative ellipticity at 208 nm (25 °C), no simple correlation of ellipticity with either transition temperature or Trp fluorescence emission maximum was present (data not shown).

Role of Aromatic Residues in Water−Membrane Interfaces. In the assessment of the critical roles of interfacial aromatic residues, both the structure of the aromatic ring and the characteristics of the lipid−water interface should be considered. The electron density of the π-system is greatest directly above and below the plane of the ring and is approaching zero in the plane of the ring, imparting to the ring a permanent quadrupole moment (*51*), and accordingly the innate ability to participate in a variety of polar interactions, including strong cation−π (*51*, *52*), oxygen−aromatic (*53*), sulfur−aromatic (*54*), amino−aromatic (*55*), and aromatic−aromatic (*56*). Several such interactions are possible when Tyr, Trp, or Phe is situated at the highly heterogeneous lipid−water interface, given that the latter is about 15 Å wide on each side of the membrane, and contains a complex mixture of components, such as methylene groups, carbonyl groups, glycerol, phosphate groups, lipid headgroups, and water (*57*, *58*). The ability of the interfacial region to accommodate aromatic rings is reinforced by the top rankings of aromatic residues in hydrophobicity scales developed from the propensities of peptides to transfer from water to a hydrophobic phase (*47*, *48*). In this context, our work established that viable mutants of the protein could not be generated with both Tyr-21 and Tyr-24 simultaneously mutated. Among the virtually identical major coat proteins of phages M13, fd and f1, the only literature report of such a double-site mutant is Y21F/Y24S in bacteriophage f1 (*59*), which nevertheless still retains one aromatic residue. The absence of such "double-site aromatic knockout" mutants makes it tempting to suggest that Tyr-21 and Tyr-24, likely in combination with the nonmutable Trp-26, are vital for the positional anchoring of the protein. Such anchoring must thus require the specific presence of π-electron character for protein segments in the interface, which, in contrast to purely aliphatic character, maintains the capacity to form and stabilize essential interactions with one or more of the polar substituents presented to the protein by this region of the phospholipid membrane. Amphiphilic residues such as Tyr and Trp may be particularly suited for interfacial positioning, as they can effectively bridge the two contrasting environments during protein folding and assembly. The results presented here highlight the subtle role of persistent interfacial aromatic character (two out of three residues) in producing the optimal (WT) structure. One could envision a "push−pull" role for interfacial Tyr residues in fine-tuning the positions of both the N-terminal and TM helices vis-à-vis the surface of the membrane particle.

In any analysis of the structural and biological roles of the interfacial aromatic residues in M13 major coat protein, it should be recalled that the protein must adapt to two very different environments during the phage life cycle: when in the membrane during viral infection of *E. coli* and when interacting with other protein monomers in the virion as a DNA-binding protein. The relatively small size of this protein implies that many, if not all, residues need to assume dual or even multiple functions to ensure the structural stability of the protein in the two environments as well as to maintain some flexibility to allow a smooth transition between the two forms. For example, it has been shown that the three Phe residues (from different protein subunits) form a cluster of stacked phenyl rings in the virion which is critical for the latter's integrity (*60*, *61*). Trp-26 (from yet another subunit) may participate in the stabilization of this cluster (*62*). However, as noted above, four of the six positions with aromatic residues in M13 coat protein (Phe-11, Trp-26, Phe-42, and Phe-45) are essentially fully resistant to mutation; indeed, no mutants of Trp-26, Phe-42, and Phe-45 have yet been observed, and the only reported viable mutant at Phe-11 is F11Y (*60*), which still retains an aromatic ring.

Recognizing that the mutants that were obtained are limited by the requirement that they must not be lethal to phage viability, we note that largely polar mutations were obtained at Tyr-24 but largely nonpolar mutations at Tyr-21. As the results from spectral studies suggest that polar Y24 mutants tend to move the protein away from the membrane core, one can attribute a primary interfacial anchoring function to the Tyr-21 position, with the strong possibility that its side chain dips directly into the membrane nonpolar region. This latter suggestion is supported by the fact that the transition temperature for Y21F, a less polar mutant than the wild type Y, increases by 2−3 °C. Thus, it seems that wild type Tyr is a "de-optimized" yet functional choice for maintenance of the dynamics required during the phage life cycle.

CONCLUSION

Using a series of M13 major coat protein mutants in deoxycholate micelles as a model protein−lipid system, we have shown that the positioning of the effective TM segment and the strength of the lipid−protein interactions are measurably affected by the replacement of either the interfacial Tyr-21 or Tyr-24 residue of the protein. The fact that substitutions of Tyr with residues with varying polarity within the N-terminal membrane−water interfacial region of the protein−micelle system led to a significant range in thermally induced $\alpha \rightarrow \beta$ transitions may indicate that the wild type Tyr residues have been chosen for participation directly in an anchoring function. The overall results suggest that an interfacial Tyr is a primary recognition element for precise strand positioning in vivo, a function that apparently cannot be performed by residues with simple aliphatic character.

ACKNOWLEDGMENT

We thank Dr. Avijit Chakrabartty for use of the fluorescence spectrometer in his laboratory, Dr. Tuhina Neogi for initial generation of several Y21 mutants, and Dr. Reinhart Reithmeier and Ms. Chen Wang for helpful discussions.

REFERENCES

1. Tsang, S., and Saier, M. H., Jr. (1996) *J. Comput. Biol. 3*, 185−190.
2. Espanol, M. J., and Saier, M. H., Jr. (1995) *Mol. Membr. Biol. 12*, 193−200.
3. Sipos, L., and von Heijne, G. (1993) *Eur. J. Biochem. 213*, 1333−1340.
4. Reithmeier, R. A. F. (1995) *Curr. Opin. Struct. Biol. 5*, 491−500.
5. Deisenhofer, J., and Michel, H. (1989) *Science 245*, 1463−1473.

6. Doyle, D. A., Cabral, J. M., Pfuetzner, R. A., Kuo, A., Gulbis, J. M., Cohen, S. L., Chait, B. T., and MacKinnon, R. (1998) *Science 280*, 69−77.
7. Cowan, S. W., Schirmer, T., Rummel, G., Steiert, M., Ghosh, R., Pauptit, R. A., Jansonius, J. N., and Rosenbusch, J. P. (1992) *Nature 358*, 727−733.
8. Landolt-Marticorena, C., Williams, K. A., Deber, C. M., and Reithmeier, R. A. F. (1993) *J. Mol. Biol. 229*, 602−608.
9. Pawagi, A. B., and Deber, C. M. (1990) *Biochemistry 29*, 950−955.
10. Schiffer, M., Chang, C.-H., and Stevens, F. J. (1992) *Protein Eng. 5*, 213−214.
11. Braun, P., and von Heijne, G. (1999) *Biochemistry 38*, 9778−9782.
12. Rasched, I., and Oberer, E. (1986) *Microbiol. Rev. 50*, 401−427.
13. Model, P., and Russel, M. (1988) in *The Bacteriophages* (Calendar, R., Ed.) pp 375−456, Plenum Press, New York.
14. Webster, R. E. (1996) in *Phage Display of Peptides and Proteins: A Laboratory Manual* (Kay, B. K., Winter, J., and McCafferty, J., Eds.) pp 1−20, Academic Press, San Diego.
15. Makowski, L., and Russel, M. (1997) in *Structural Biology of Viruses* (Chiu, W., Burnett, R. M., and Garcea, R. L., Eds.) pp 352−380, Oxford University Press, New York.
16. Marvin, D. A. (1998) *Curr. Opin. Struct. Biol. 8*, 150−158.
17. van Wezenbeek, P. M. G. F., Hulsebos, T. J. M., and Schoenmakers, J. G. G. (1980) *Gene 11*, 129−148.
18. Berkowitz, S. A., and Day, L. A. (1976) *J. Mol. Biol. 102*, 531−547.
19. Nozaki, Y., Chamberlain, B. K., Webster, R. E., and Tanford, C. (1976) *Nature 259*, 335−337.
20. Wickner, W. (1976) *Proc. Natl. Acad. Sci. U.S.A. 73*, 1159−1163.
21. Henry, G. D., and Sykes, B. D. (1992) *Biochemistry 31*, 5284−5297.
22. McDonnell, P. A., Shon, K., Kim, Y., and Opella, S. J. (1993) *J. Mol. Biol. 233*, 447−463.
23. Spruijt, R. B., Wolfs, C. J. A. M., Verver, J. W. G., and Hemminga, M. A. (1996) *Biochemistry 35*, 10383−10391.
24. Stopar, D., Spruijt, R. B., Wolfs, C. J. A. M., and Hemminga, M. A. (1996) *Biochemistry 35*, 15467−15473.
25. Papavoine, C. H. M., Christiaans, B. E. C., Folmer, R. H. A., Konings, R. N. H., and Hilbers, C. W. (1998) *J. Mol. Biol. 282*, 401−419.
26. Li, Z., and Deber, C. M. (1991) *Biochem. Biophys. Res. Commun. 180*, 687−693.
27. Williams, K. A., Glibowicka, M., Li, Z., Li, H., Khan, A. R., Chen, Y. M. Y., Wang, J., Marvin, D. A., and Deber, C. M. (1995) *J. Mol. Biol. 252*, 6−14.
28. Rychlik, W., Spencer, W. J., and Rhoads, R. E. (1990) *Nucleic Acids Res. 18*, 6409−6412.
29. Sayers, J. R., Krekel, C., and Eckstein, F. (1992) *BioTechniques 13*, 592−596.
30. Deber, C. M., Khan, A. R., Li, Z., Joensson, C., Glibowicka, M., and Wang, J. (1993) *Proc. Natl. Acad. Sci. U.S.A. 90*, 11648−11652.
31. Haigh, N. G., and Webster, R. E. (1998) *J. Mol. Biol. 279*, 19−29.
32. Spruijt, R. B., and Hemminga, M. A. (1991) *Biochemistry 30*, 11147−11154.
33. Schmid, F. X. (1989) in *Protein Structure: A Practical Approach* (Creighton, T. E., Ed.) pp 251−285, IRL Press, Oxford, United Kingdom.
34. Eftink, M. R., and Ghiron, C. A. (1981) *Anal. Biochem. 114*, 199−227.
35. Lakowicz, J. R. (1983) *Principles of Fluorescence Spectroscopy*, Plenum Press, New York.
36. Henry, G. D., Weiner, J. H., and Sykes, B. D. (1986) *Biochemistry 25*, 590−598.
37. Makino, S., Woolford, J. L., Jr., Tanford, C., and Webster, R. E. (1975) *J. Biol. Chem. 250*, 4327−4332.
38. Stopar, D., Spruijt, R. B., Wolfs, C. J. A. M., and Hemminga, M. A. (1998) *Biochemistry 37*, 10181−10187.
39. Small, D. M. (1971) in *The Bile Acids: Chemistry, Physiology, and Metabolism, Vol. 1: Chemistry* (Nair, P. P., and Kritchevsky, D., Eds.) pp 249−356, Plenum Press, New York.
40. Helenius, A., McCaslin, D. R., Fries, E., and Tanford, C. (1979) *Methods Enzymol. 56*, 734−749.
41. D'Alagni, M., D'Archivio, A. A., Galantini, L., and Giglio, E. (1997) *Langmuir 13*, 5811−5815.
42. Chakrabartty, A., Kortemme, T., Padmanabhan, S., and Baldwin, R. L. (1993) *Biochemistry 32*, 5560−5565.
43. Hemminga, M. A., Sanders, J. C., and Spruijt, R. B. (1992) *Prog. Lipid Res. 31*, 301−333.
44. Li, Z., Glibowicka, M., Joensson, C., and Deber, C. M. (1993) *J. Biol. Chem. 268*, 4584−4587.
45. Laidler, K. J., and Meiser, J. H. (1995) *Physical Chemistry*, 2nd ed., Houghton Mifflin Company, Boston.
46. Kyte, J., and Doolittle, R. F. (1982) *J. Mol. Biol. 157*, 105−132.
47. Wimley, W. C., and White, S. H. (1996) *Nat. Struct. Biol. 3*, 842−848.
48. Liu, L.-P., and Deber, C. M. (1998) *Biopolymers 47*, 41−62.
49. Tory, M. C., and Merrill, A. R. (1999) *J. Biol. Chem. 274*, 24539−24549.
50. Engelman, D. M., Steitz, T. A., and Goldman, A. (1986) *Annu. Rev. Biophys. Biophys. Chem. 15*, 321−353.
51. Dougherty, D. A. (1996) *Science 271*, 163−168.
52. Mecozzi, S., West, A. P., Jr., and Dougherty, D. A. (1996) *Proc. Natl. Acad. Sci. U.S.A. 93*, 10566−10571.
53. Burley, S. K., and Petsko, G. A. (1988) *Adv. Protein Chem. 39*, 125−189.
54. Reid, K. S. C., Lindley, P. F., and Thornton, J. M. (1985) *FEBS Lett. 190*, 209−213.
55. Burley, S. K., and Petsko, G. A. (1986) *FEBS Lett. 203*, 139−143.
56. Hunter, C. A., Singh, J., and Thornton, J. M. (1991) *J. Mol. Biol. 218*, 837−846.
57. Wiener, M. C., and White, S. H. (1992) *Biophys. J. 61*, 434−447.
58. White, S. H. (1994) in *Membrane Protein Structure: Experimental Approaches* (White, S. H., Ed.) pp 97−124, Oxford University Press, New York.
59. Overman, S. A., Aubrey, K. L., Vispo, N. S., Cesareni, G., and Thomas, G. J., Jr. (1994) *Biochemistry 33*, 1037−1042.
60. Marvin, D. A., Hale, R. D., Nave, C., and Helmer Citterich, M. (1994) *J. Mol. Biol. 235*, 260−286.
61. Matsuno, M., Takeuchi, H., Overman, S. A., and Thomas, G. J., Jr. (1998) *Biophys. J. 74*, 3217−3225.
62. Arnold, G. E., Day, L. A., and Dunker, A. K. (1992) *Biochemistry 31*, 7948−7956.
63. Williams, K. A., Farrow, N. A., Deber, C. M., and Kay, L. E. (1996) *Biochemistry 35*, 5145−5157.

BI0016117